Journal of *Marine Science and Engineering*

MDPI

Article

Theoretical and Numerical Analysis of Blasting Pressure of Cylindrical Shells under Internal Explosive Loading

Zhan-Feng Chen [1,2], Hui-Jie Wang [1], Zhiqian Sang [1,*], Wen Wang [1], He Yang [1], Wei-Ming Meng [3] and Yu-Xing Li [2,*]

[1] School of Mechanical Engineering, Hangzhou Dianzi University, Hangzhou 310018, China; czf@hdu.edu.cn (Z.-F.C.); whj@hdu.edu.cn (H.-J.W.); wangwn@hdu.edu.cn (W.W.); yanghe@hdu.edu.cn (H.Y.)
[2] Provincial Key Laboratory of Oil and Gas Storage and Transportation Safety in Shandong Province, University of Petroleum (Huadong), Qingdao 266580, China
[3] Qingdao Hisense Electronic Technology Service Co., Ltd., Qingdao 266001, China; mengweiming@hisense.com
* Correspondence: sang@hdu.edu.cn (Z.S.); liyx@upc.edu.cn (Y.-X.L.)

Abstract: Cylindrical shells are principal structural elements that are used for many purposes, such as offshore, sub-marine, and airborne structures. The nonlinear mechanics model of internal blast loading was established to predict the dynamic blast pressure of cylindrical shells. However, due to the complexity of the nonlinear mechanical model, the solution process is time-consuming. In this study, the nonlinear mechanics model of internal blast loading is linearized, and the dynamic blast pressure of cylindrical shells is solved. First, a mechanical model of cylindrical shells subjected to internal blast loading is proposed. To simplify the calculation, the internal blast loading is reduced to linearly uniform variations. Second, according to the stress function method, the dynamic blast pressure equation of cylindrical shells subjected to blast loading is derived. Third, the calculated results are compared with those of the finite element method (FEM) under different durations of dynamic pressure pulse. Finally, to reduce the errors, the dynamic blast pressure equation is further optimized. The results demonstrate that the optimized equation is in good agreement with the FEM, and is feasible to linearize the internal blast loading of cylindrical shells.

Keywords: internal blast loading; linearization; dynamic blast pressure; cylindrical shells; analytical solution

Citation: Chen, Z.-F.; Wang, H.-J.; Sang, Z.; Wang, W.; Yang, H.; Meng, W.-M.; Li, Y.-X. Theoretical and Numerical Analysis of Blasting Pressure of Cylindrical Shells under Internal Explosive Loading. *J. Mar. Sci. Eng.* **2021**, *9*, 1297. https://doi.org/10.3390/jmse9111297

Academic Editors: José A. F. O. Correia and Franck Schoefs

Received: 20 September 2021
Accepted: 17 November 2021
Published: 19 November 2021

1. Introduction

Cylindrical shells are special pressure vessels that are widely used in offshore and sub-marine structures, among others. In offshore applications, the cylindrical shell structures are utilized to transport oil and gas [1]. In sub-marine applications, the pressure shell is the primary element for withstanding diving pressure [2]. To solve explosion problems of cylindrical shells, scholars often simplify the blast loadings into nonlinear loads via theoretical analysis [3] and finite element simulation [4]; however, the nonlinear load model of the internal blast loading is complicated, and its solution is difficult and time-consuming. Therefore, it is necessary to establish a more effective model to solve the problem.

The interaction between explosion products and containers is one of the topics in the research of cylindrical shells. Scholars have carried out research by means of theoretical analysis, blasting tests, and numerical simulations [5,6]. In 1958, Baker and Allen [7] first established a general response theory for spherical shells of arbitrary thickness, showing that even "thin-shell" equations of motion can accurately describe relatively thick shells. In 1960, Baker [8] proposed a theory for predicting the elastic–plastic response of thin spherical shells subjected to transient loads. Duffey et al. [9] studied the approximate expression of the ultimate circumferential strain (or radial displacement) versus the axial

coordinates of a cylindrical shell, when a spherical explosive charge was loaded at the center. Ko et al. [10] analyzed the dynamic response of a multilayer spherical container made of the same material and thickness subjected to intermittent internal explosive loads. Karpp et al. [11] discussed the response of steel containment to the explosive load of high explosives. Ruiz et al. [12] calculated the strength of thin-walled cylindrical shells subjected to explosive loads. Ma et al. [13] conducted a finite element analysis of cylindrical containment shells with different crack sizes, and calculated the propagation of the cracks and the final fracture profile. Zheng et al. [14,15] examined the delamination failure of composite containers subjected to internal explosive loads. Du et al. [16,17] researched the progressive propagation of pipe cracks subjected to internal explosive loads. Chen et al. [18] simplified the blast loading as a parabolic load, and solved the dynamic blast pressure problem of cylinder shells subjected to blast loading.

Blast pressure refers to the maximum pressure that a container can withstand in bursts, and is an important parameter to evaluate the anti-explosive performance of cylindrical shells. Because an explosion is an extremely rapid physical or chemical energy-release process, the blasting of a container is classified as a dynamic mechanical behavior. However, at present, few scholars have studied the dynamic blast pressure of cylindrical shells. Our study will focus on this issue.

In this study, to simplify the calculation, the internal blast loadings are simplified to linearly varying loads. It is of great significance to simplify nonlinear load into linear load in theoretical analysis. Based on the stress function method, a dynamic blast pressure prediction formula of cylindrical shells is derived. First, a simplified model of a cylindrical shell subjected to internal explosive load is established in Section 2. Second, the components of stress and strain of cylindrical shells are obtained in Section 3, according to the stress function and boundary conditions of the cylindrical shells. Third, a dynamic blast pressure prediction equation for cylindrical shells is proposed in Section 4. Finally, the prediction equation is compared with the results of the finite element method (FEM) analysis, and the prediction equation is optimized. This study will provide an in-depth understanding of dynamic blast pressure, and will be helpful in the safety assessment and optimization design of cylindrical shells.

2. Research Model

The mechanical model describing the cylindrical shell is composed of a cylindrical surface and two hemispherical heads, as shown in Figure 1. P_i is the internal pressure on the pipeline. To simplify the calculation, it is regarded as a closed structure, ignoring openings and connectors, i.e., the model of the cylindrical shell is assumed to be an ideal cylindrical shell. The material of the cylindrical shell is also assumed to be homogeneous and isotropic.

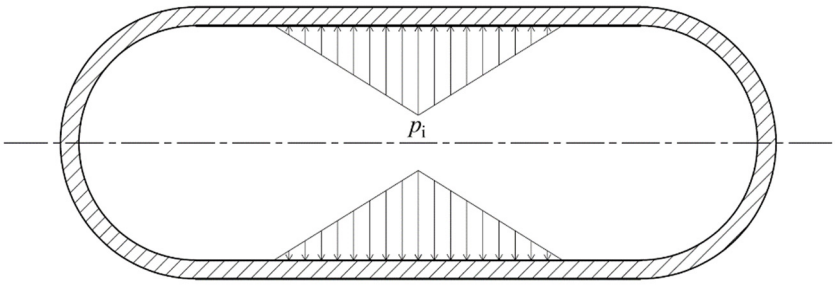

Figure 1. Geometrical model of a cylindrical shell subjected to a spindle-shaped load.

The method of center initiation [19] is usually used in experiments of explosive loading for cylindrical shells, in which trinitrotoluene (TNT) is installed in the geometric center of the cylindrical shell [20]. According to the theory of explosion dynamics, the strength of a shockwave decreases with the increase in the distance from the explosion point. In addition, deformation occurs in a limited range from the charge center along the axial direction of the shell [21]. In our mechanical model, the explosive load is approximately regarded as a spindle-shaped load. The load at the initiation point is the largest, and the load on both sides of the axial direction is inversely proportional to the distance from the initiation point. The spindle-shaped load acting on both ends of the vessel is ignored.

There is a fluid–solid coupling between the shell of the explosion vessel and the explosion flow field. The external bulging deformation of the shell reduces the wall explosion load, while the inward contraction deformation increases the wall explosion load [22]. In the theoretical model of this paper, the fluid–solid coupling, shell damage, and spindle-shaped load are not considered. The main aim of this work is to study the influence of internal spindle-shaped explosion loads on cylindrical shells. Through the analysis and calculation of the theoretical model, the dynamic blast pressure prediction equation for cylindrical shells can be obtained, which will be helpful for further study of the dynamic response of cylindrical shells subjected to internal explosion loads.

3. Theoretical Analysis

3.1. Stress Function

Although the propagation process of explosion shockwaves in cylindrical shells is complex, it is generally believed that the first shockwave plays a crucial role in the process of the cylindrical shell's deformation [8,23]. The explosion load on the inner wall of the cylindrical shell decreases with the increase in the radius of the cylindrical shell; if the explosion is at the axis, the load can be simplified as a spindle-shaped load. From the geometric characteristics of the cylindrical shell and the location of the initiation point, the boundary conditions of the cylindrical shell are axisymmetric about the z-axis, as shown in Figure 2. Therefore, the stress and strain of the cylindrical shell are also axisymmetric about the z-axis, i.e., they are the functions of r and z.

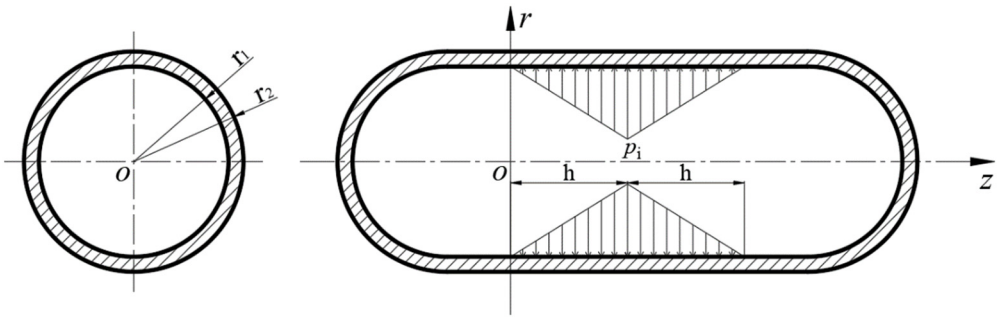

Figure 2. Model of a cylindrical shell and its spindle-shaped loadings.

The following stress function with eight undetermined coefficients is used to obtain the analytical solution [24]:

$$\phi = \gamma_1 z^4 + \gamma_2 r^4 + \gamma_3 z^3 + \gamma_4 z^2 r^2 + \gamma_5 z^2 \ln r + \gamma_6 z r^2 + \gamma_7 r^2 \ln r + \gamma_8 z \ln r \quad (1)$$

where γ_1–γ_8 are uncertainty coefficients that can be obtained from the stress/strain components of the cylindrical shell and the boundary conditions.

3.2. Stress and Displacement Component

The stress and displacement of cylindrical shells subjected to linear implosion loads can be calculated by A.E.H. Love's method. The stress components can be expressed as [24]:

$$\begin{cases} \sigma_r = \frac{\partial}{\partial z}\left(\mu\nabla^2\phi - \frac{\partial^2\phi}{\partial r^2}\right) \\ \sigma_\theta = \frac{\partial}{\partial z}\left(\mu\nabla^2\phi - \frac{1}{r}\frac{\partial\phi}{\partial r}\right) \\ \sigma_z = \frac{\partial}{\partial z}\left((2-\mu)\nabla^2\phi - \frac{\partial^2\phi}{\partial z^2}\right) \\ \tau_{rz} = \frac{\partial}{\partial z}\left((1-\mu)\nabla^2\phi - \frac{\partial^2\phi}{\partial z^2}\right) \end{cases} \tag{2}$$

The displacement components can be determined by:

$$\begin{cases} u_r = -\frac{1}{2G}\frac{\partial^2\phi}{\partial r\partial z} \\ w = \frac{1}{2G}\left[2(1-\mu)\nabla^2 - \frac{\partial^2}{\partial z^2}\right]\phi \end{cases} \tag{3}$$

In the above equation, the stress function ϕ satisfies the following biharmonic equation:

$$\nabla^2\nabla^2\phi = 0 \tag{4}$$

where ∇^2 is the three-dimensional Laplace operator. In the axisymmetric theoretical model, the Laplace operator can be expressed as:

$$\nabla^2 = \frac{\partial^2}{\partial r^2} + \frac{1}{r}\frac{\partial}{\partial r} + \frac{\partial^2}{\partial z^2} \tag{5}$$

3.3. Boundary Conditions

The boundary condition of stress and the continuity conditions of stress and strain are applied for conducting the stress and displacement of cylindrical shell. In the model shown in Figure 2, the inner radius and outer radius of the cylindrical shell are r_1 and r_2, respectively. The z-axis is along the central axis. In the cylindrical coordinate system, p_1 and p_2 are assumed to be the internal and external radial constant pressures. The action position of the explosive load inside the cylindrical shell is from 0 to $2h$. Because the internal explosion load is symmetrical about the r-axis, in order to simplify the calculation, the linear load of the cylindrical shell in this paper is from 0 to h on the z-axis. k_1 and k_2 are the gradients of pressure along the axis for the internal and the external walls, respectively. The load boundary conditions of the cylindrical shell are as follows:

$$\begin{cases} r = r_1 : \sigma_r = k_1 z + p_1, \tau_{rz} = 0 \\ r = r_2 : \sigma_r = k_2 z + p_2, \tau_{rz} = 0 \\ z = 0, h : \sigma_z = q, \tau_{rz} = 0 \end{cases} \tag{6}$$

3.4. Solving the Stress Function

The uncertainty coefficients can be determined from the stress/strain components and the boundary conditions of the cylindrical shell. Afterwards, the stress and strain components of the cylindrical shell can be obtained.

Substituting Equation (1) into Equation (2) yields:

$$\begin{cases} \sigma_r = [24\mu\gamma_1 + 4(2\mu-1)\gamma_4]z + 2\gamma_5 z/r^2 + \gamma_8/r^2 + 6\mu\gamma_3 + 2(2\mu-1)\gamma_6 \\ \sigma_\theta = [24\mu\gamma_1 + 4(2\mu-1)\gamma_4]z - 2\gamma_5 z/r^2 - \gamma_8/r^2 + 6\mu\gamma_3 + 2(2\mu-1)\gamma_6 \\ \sigma_z = [24(1-\mu)\gamma_1 + 8(2-\mu)\gamma_4]z + 6(1-\mu)\gamma_3 + 4(2-\mu)\gamma_6 \\ \tau_{rz} = [32(1-\mu)\gamma_2 - 4\mu\gamma_4]r + [4(1-\mu)\gamma_7 - 2\mu\gamma_5]/r \end{cases} \tag{7}$$

By substituting Equation (7) into Equation (6):

$$\gamma_1 = \frac{2-\mu}{12(1+\mu)} \frac{k_2 {r_2}^2 - k_1 {r_1}^2}{({r_2}^2 - {r_1}^2)} \tag{8}$$

$$\gamma_2 = -\frac{\mu}{32(1+\mu)} \frac{k_2 {r_2}^2 - k_1 {r_1}^2}{({r_2}^2 - {r_1}^2)} \tag{9}$$

$$\gamma_3 = -\frac{2-\mu}{3(1+\mu)} \frac{p_2 {r_2}^2 - p_1 {r_1}^2}{{r_2}^2 - {r_1}^2} + \frac{1-2\mu}{6(1+\mu)} q \tag{10}$$

$$\gamma_4 = -\frac{1-\mu}{4(1+\mu)} \frac{k_2 {r_2}^2 - k_1 {r_1}^2}{({r_2}^2 - {r_1}^2)} \tag{11}$$

$$\gamma_5 = -\frac{{r_1}^2 {r_2}^2 (k_2 - k_1)}{2({r_2}^2 - {r_1}^2)} \tag{12}$$

$$\gamma_6 = \frac{1-\mu}{2(1+\mu)} \frac{p_2 {r_2}^2 - p_1 {r_1}^2}{{r_2}^2 - {r_1}^2} + \frac{\mu}{2(1+\mu)} q \tag{13}$$

$$\gamma_7 = -\frac{\mu}{1-\mu} \frac{{r_1}^2 {r_2}^2 (k_2 - k_1)}{4({r_2}^2 - {r_1}^2)} \tag{14}$$

$$\gamma_8 = \frac{{r_1}^2 {r_2}^2 (p_2 - p_1)}{{r_2}^2 - {r_1}^2} \tag{15}$$

By substituting the coefficients ($\gamma_1 \sim \gamma_8$) into Equation (7):

$$\begin{cases} \sigma_r = \frac{(p_2+k_2 z) r_2^2 (-r^2+r_1^2) + (p_1+k_1 z) r_1^2 (r^2-r_2^2)}{r^2 (r_1^2 - r_2^2)} \\ \sigma_\theta = \frac{-(p_2+k_2 z) r_2^2 (r^2+r_1^2) + (p_1+k_1 z) r_1^2 (r^2+r_2^2)}{r^2 (r_1^2 - r_2^2)} \\ \sigma_z = q \\ \tau_{rz} = 0 \end{cases} \tag{16}$$

By substituting the undetermined coefficient(s) ($\gamma_1 \sim \gamma_8$) and Equation (1) into Equation (3), the displacement components of cylindrical shells can be obtained:

$$\begin{cases} u_r = \frac{1}{2G}\left[\left(\frac{1-\mu}{1+\mu}\Delta_1 r + \Delta_3 \frac{1}{r}\right) z - \left(\frac{1-\mu}{1+\mu}\Delta_2 r + \Delta_4 \frac{1}{r}\right)\right] - \frac{\mu r q}{E} \\ w = -\frac{1}{2G}\left[-\frac{\mu}{1+\mu}\Delta_1 z^2 + \frac{\mu-1}{2(1+\mu)}\Delta_1 r^2 + \frac{2\mu}{1+\mu}\Delta_2 z - \Delta_3 \ln r - 2\mu\Delta_3\right] + \frac{qz}{E} \end{cases} \tag{17}$$

where $\Delta_1 = \frac{k_2 {r_2}^2 - k_1 {r_1}^2}{{r_2}^2 - {r_1}^2}$, $\Delta_2 = \frac{p_2 {r_2}^2 - p_1 {r_1}^2}{{r_2}^2 - {r_1}^2}$, $\Delta_3 = \frac{{r_1}^2 {r_2}^2 (k_2 - k_1)}{{r_2}^2 - {r_1}^2}$ and $\Delta_4 = \frac{{r_1}^2 {r_2}^2 (p_2 - p_1)}{{r_2}^2 - {r_1}^2}$.

4. Dynamic Blast Pressure

Barsom and Rolfe [25] classified loads into two types: static and quasi-static loads, and dynamic loads. A load with a strain rate of less than 10^{-5} is regarded as a static or quasi-static load; steady-state, creep, and relaxation loads are generally in this type. A load with a strain rate from 10^{-2} to 10^{6} is regarded as a dynamic load. For traffic and machinery, the strain rate is usually between 10^{-2} and 10^{-1}; for earthquakes and cranes, the strain rate is usually between 10^{-1} and 10^{1}; and for explosions and blast loads, the strain rate is usually between 10^{1} and 10^{6}. Since the 1940s, many scholars have studied the bearing capacity of cylindrical shells subjected to static and quasi-static loads. The equations for blast pressure prediction are shown in Table 1. Additionally, previous studies on pipelines with corrosion and wear defects by the author of this paper revealed several static blasting pressure equations [26–29]. However, because the blast pressure is a typical high-strain-rate load [30], these static blast pressure prediction equations cannot accurately predict the blast pressure of a cylindrical shell subjected to an internal explosive load. In this paper, the explosive load undertaken by the cylindrical shell changes with time.

Table 1. Representative predictive formulae for blast pressure (P_b), reproduced from [26], with permission from Elsevier, 2021.

Contributor	Equation	Contributor	Equation
Faupel	$P_b = \frac{2}{\sqrt{3}}\sigma_b(2-\frac{\sigma_y}{\sigma_b})\ln(k)$	Turner	$P_b = \sigma_b \ln(k)$
API	$P_b = 0.875(\frac{2\sigma_y T}{D})$	ASME	$P_b = \sigma_b(\frac{k-1}{0.6k+0.4})$
Nadai (1)	$P_b = \frac{2}{\sqrt{3}}\sigma_b \ln(k)$	Maximum shear stress	$P_b = 2\sigma_b(\frac{k-1}{k+1})$
Nadai (2)	$P_b = \frac{\sigma_b}{\sqrt{3n}}(1-\frac{1}{k^{2n}})$	Baily–Nadai	$P_b = \frac{2\sigma_b t}{D-t}\left[\left(\frac{1}{2}\right)^{1+n}+\left(\frac{1}{\sqrt{3}}\right)^{1+n}\right]$
Soderberg	$P_b = \frac{4}{\sqrt{3}}\sigma_b(\frac{k-1}{k+1})$	Klever	$P_b = \left(\frac{2+\sqrt{3}}{4\sqrt{3}}\right)^n \frac{4T\sigma_b}{D_m}$
Maximum stress	$P_b = \sigma_b(k-1)$	Zhu–Leis	$P_b = \frac{2}{\sqrt{3}}\sigma_b(2-\frac{\sigma_y}{\sigma_b})\ln(k)$

In our model, the explosion load inside the cylindrical shell is simplified to a spindle-shaped load, as shown in Equation (6). It can be seen from Figure 2 that the explosive load of the cylindrical shell is the greatest when $z = h$ and $r = r_1$, and the stress of the cylindrical shell is the greatest at the same point. Therefore, by substituting $p_2 = 0$, $z = h$, and $r = r_1$ into Equation (16), the stress component can be obtained as follows:

$$\begin{cases} \sigma_r = p_i \\ \sigma_\theta = \frac{p_i({r_1}^2+{r_2}^2)}{{r_2}^2-{r_1}^2} \\ \sigma_z = q \\ \tau_{rz} = 0 \end{cases} \tag{18}$$

Once the hoop stress reaches the ultimate tensile strength, the cylindrical shell will burst:

$$\sigma_\theta = \frac{p_i({r_1}^2+{r_2}^2)}{{r_2}^2-{r_1}^2} = \sigma_b \tag{19}$$

From Figure 2, p_i is the maximum explosive load inside the cylindrical shell. Therefore, according to Equation (19), the static blast pressure can be expressed as follows:

$$\begin{aligned} p_i &= p_b^s \\ &= \frac{{r_2}^2-{r_1}^2}{{r_1}^2+{r_2}^2}\sigma_b \end{aligned} \tag{20}$$

The dynamic explosion pressure of the cylindrical shell changes with time [31]; therefore, the inertial effect produced cannot be ignored. Unlike static ultimate tensile strength, dynamic ultimate tensile strength is also related to time. In 1980, Baker et al. discussed the relationship between dynamic and static ultimate tensile strength [32]. The dynamic ultimate tensile strength can be derived from the static ultimate tensile strength and strain rate as follows:

$$\sigma_b^d = \sigma_b\left[1.1 + 0.1\log\left(\dot{\varepsilon}\cdot s\right)\right] \tag{21}$$

where σ_b^d is the dynamic ultimate tensile strength, σ_b is the static ultimate tensile strength, $\dot{\varepsilon}$ is the strain rate, $\dot{\varepsilon} = \varepsilon/t_b$, ($t_b$ is the burst time), and s is the time in seconds.

Substituting Equation (21) into Equation (20), the dynamic blast pressure prediction equation can be taken as:

$$p_b^d = \frac{{r_2}^2 - {r_1}^2}{{r_1}^2 + {r_2}^2}\sigma_b\left[1.1 + 0.1\log\left(\dot{\varepsilon}\cdot s\right)\right] \tag{22}$$

5. Finite Element Analysis

With the development of modern numerical simulation and high-speed computer technologies, the dynamic response of vessel structures subjected to explosion loads can be accurately simulated by numerical simulation technology, which is now an important means of studying the above problems. In this paper, finite element analysis results from the literature [33] are used to verify the accuracy of the dynamic blast pressure prediction Equation (22). In the literature [33], the blast pressure of a cylindrical metal shell subjected to short-term dynamic loading was analyzed by using the general explicit dynamic analysis program LS-DYNA. The details are as follows:

5.1. Geometry and Material Data

Figure 3 demonstrates the shape and dimensions of the cylindrical shell, which consists of a cylindrical shell and two hemispherical covers at the ends; r_1 and r_2 are the inner and outer radius of the cylindrical shell, respectively. In addition, any defect is ignored in the geometric model. The material of the cylindrical shell analyzed in the literature was ASTM A-106 B steel; this type of steel also contains other elements, including C (0.17%), Mn (0.77%), P (0.010%), S (0.025%), and Si (0.25%). ASTM A-106 B steel corresponds to "MAT Type 24, piecewise linear isotropic plasticity model" in LS-DYNA. This material model can reflect the elastic–plastic properties of materials.

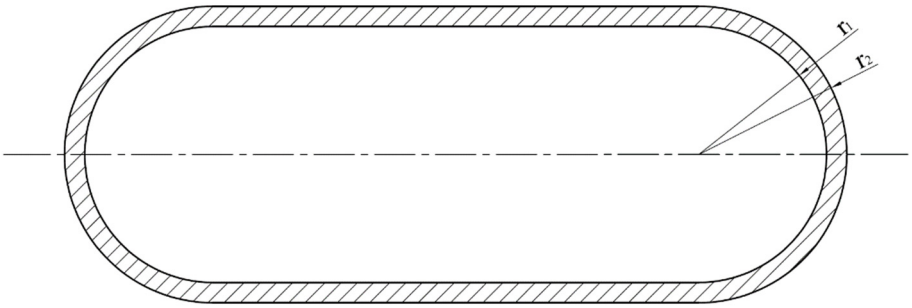

Figure 3. Shape and dimensions of the cylindrical shell.

5.2. Loading and Boundary Conditions

The loading and boundary conditions of cylindrical shells are symmetrical. In the literature, a series of pressure–time history curves similar to those of water hammer were defined and input into the finite element model to define the load on the cylindrical shell. The duration of half of the pressure pulse period is from 3.9 ms to 390 ms. During the trial process, the minimum dynamic blast pressure caused by one loading step is determined by

the highest peak pressure. The boundary conditions are shown in Figure 4. The gravity of the cylindrical shell acts on the negative direction of the y-axis, and the end of the sealing cap is fixed along the y-axis; however, there is no rotation constraint.

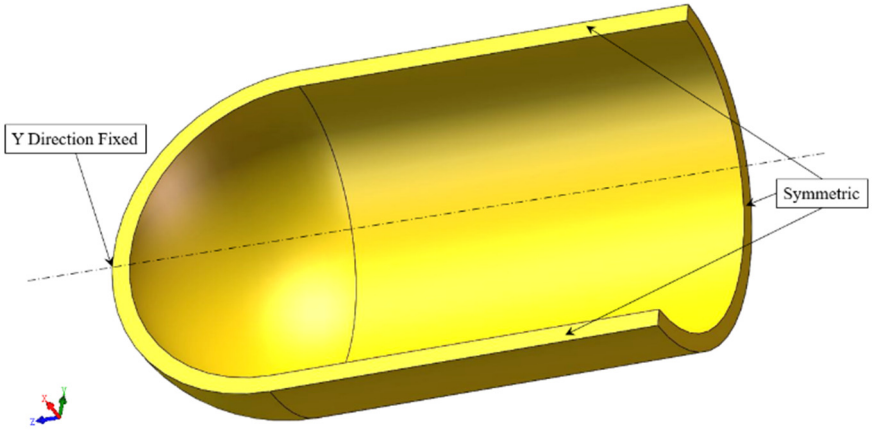

Figure 4. Boundary conditions of the finite element model.

5.3. Finite Element Analysis Results

The geometric structure and the load of the cylindrical shell are axisymmetric. To reduce computational cost, 1/4 models shown in Figure 5 are established for the finite element analysis. Through mesh sensitivity analysis, the size and number of elements of the model are determined, and the influence of different modeling parameters on the prediction of burst pressure is minimized. In this finite element model, the length (excluding the caps) is double the outer diameter of the cylindrical shell. The element type adopts eight node hexahedral elements, the aspect ratio is 1.35, the inner layer has 35 elements along the half-circumference, and the span of each element is ~5.1°. The blast failure criterion of the finite element analysis is based on the maximum plastic strain at different strain rates. Under the action of load, when the plastic strain of the element reaches the preset maximum value, the element is considered to be invalid, and is subsequently deleted. When the element is deleted, it means that the cylindrical shell has burst. In the output file of the finite element analysis, the time and pressure of the blast are recorded. The results are listed in Appendix A.

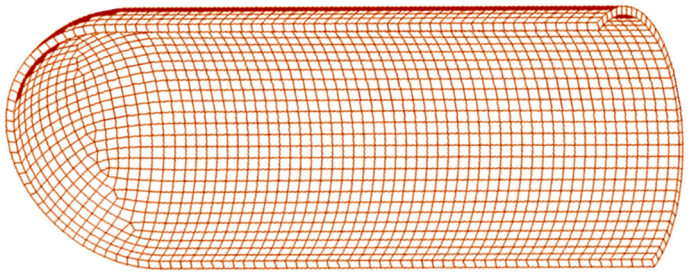

Figure 5. The finite element model.

6. Results and Discussion

6.1. Advantages and Disadvantages of the Proposed Model

In this paper, the explosive load was simplified to be a linear load. Then, the dynamic blast pressure prediction equation of the cylindrical shell was obtained based on the stress function and the explosive load boundary conditions. The ultimate bearing capacity of cylindrical shells—an important parameter of pressure vessels—was studied. There are two main advantages of this research: The first lies in the simplification of the explosive load, whereby the explosive load is treated as spindle-shaped load—a linear load. The

second advantage is due to the inherent characteristics of the developed dynamic blast pressure equation for the cylindrical shell subjected to a spindle-shaped explosive load. The equation is novel, but has shortcomings. First, to simplify the calculation, the fluid–solid coupling behavior during the explosion is ignored. Second, the effect of the heat and solid products from the explosion on the cylindrical shell is not considered. This paper focuses only on the dynamic blast pressure prediction equation of the cylindrical shell subjected to an internal explosive load.

6.2. Comparison with the FEM Results

When the cylindrical shell is subjected to explosive load until burst, the spike duration of dynamic pressure pulse t_d will be shorter than the dynamic burst time t_b. The latter is recorded in the solution output file, and can be obtained by post-processing, as shown in Appendix A. The maximum dynamic strain ε of ASTM A-106B steel is 0.262, and its static ultimate tensile strength σ_b is 413.7 MPa. Substituting these parameters into Equation (22), the dynamic blast pressure of the cylindrical shell can be calculated.

Figures 6–8 show the comparison between the FEM analysis results and the predicted values of dynamic blast pressure obtained by Equation (22) when t_d is 3.9 ms, 39 ms, and 390 ms, respectively. Figures 6–8 contain 16 cases for comparison. The parameters that determine the comparison results are in Tables A1–A3 of Appendix A, while Figures 6–8 only show the comparison results. In Figure 6, compared with the results of FEM analysis, the maximum and minimum errors of Equation (22) are 26.48% and 18.37%, respectively. In Figure 7, compared with the results of FEM analysis, the maximum and minimum errors of Equation (22) are 16.66% and 13.24%, respectively. In Figure 8, compared with FEM analysis results, the maximum and minimum errors of Equation (22) are −3.99% and −2.09%, respectively. When the timestep of the finite element analysis is determined, if the dynamic pressure pulse duration t_d is smaller, the accuracy of the finite element analysis is also lower. The results show that there is a gap between the dynamic blast pressure calculated from Equation (22) and the FEM results, which cannot meet the engineering requirements well.

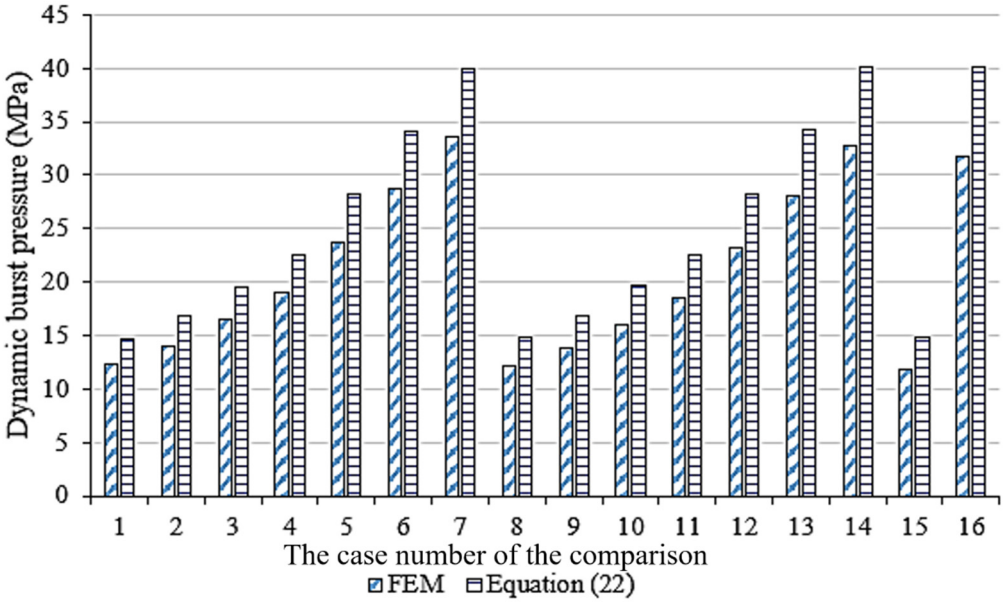

Figure 6. Comparisons between the FEM results and Equation (22), when t_d = 3.9 ms.

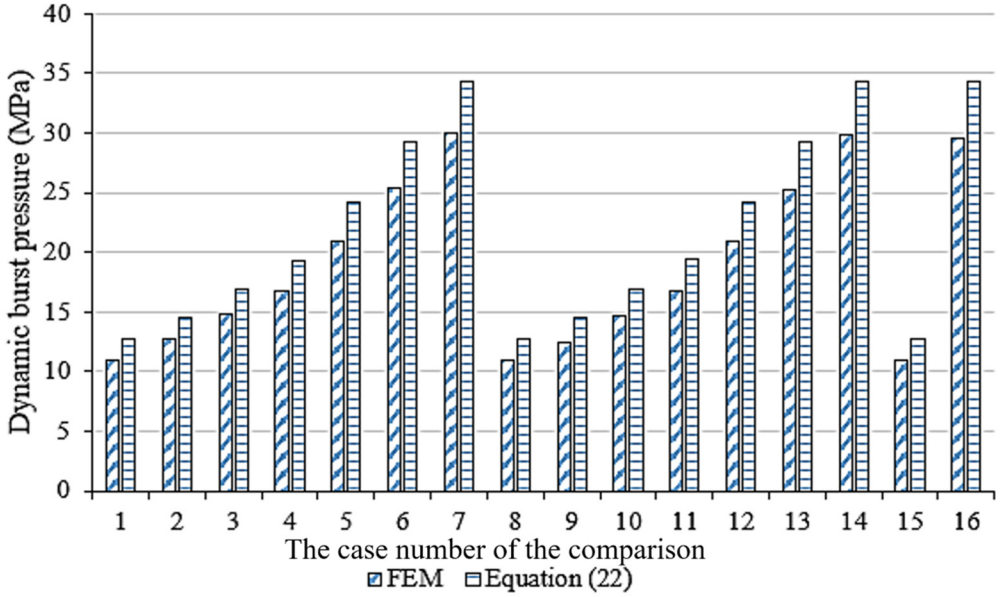

Figure 7. Comparisons between the FEM results and Equation (22), when t_d = 39 ms.

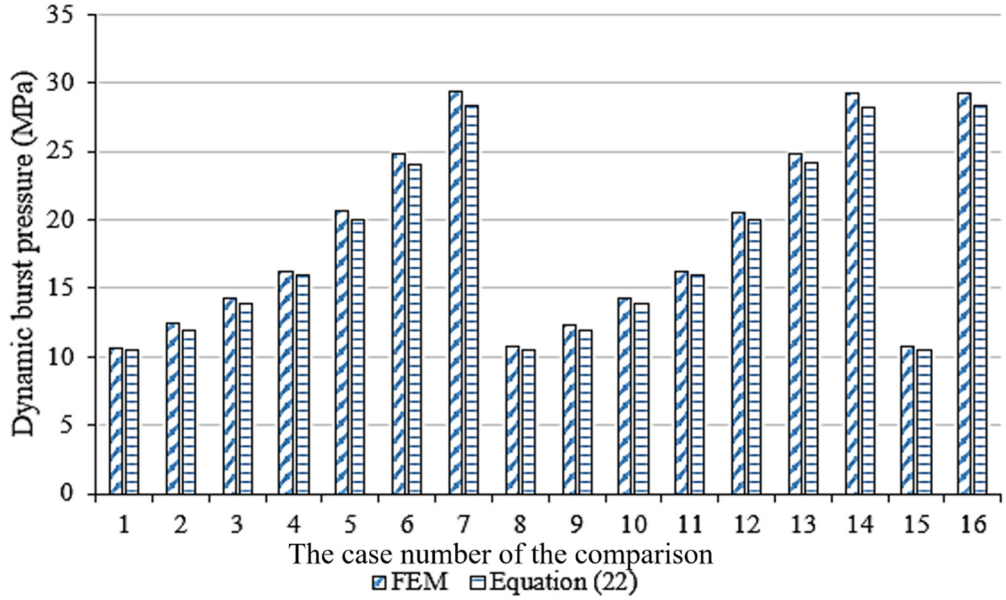

Figure 8. Comparisons between the FEM results and Equation (22), when t_d = 390 ms.

6.3. Optimization of the Prediction Equation

The optimization of dynamic blast pressure equation starts from the dynamic pressure pulse duration. According to Figures 6–8, when the dynamic pressure pulse duration t_d is shorter, the error of the predictive equation becomes larger. Therefore, a modified function is proposed to make the prediction of the dynamic blast pressure p_d more consistent with the FEM. The expression of the modified function is as follows:

$$f(t_b) = at_b{}^2 + bt_b + c \tag{23}$$

According to the regression analysis, the undetermined coefficients can be determined as $a = -0.0000029$, $b = 0.0018$, and $c = 0.8$. Therefore, the optimized dynamic blast pressure equation can be expressed as:

$$\begin{aligned} p_b^d &= f(t_b)\frac{{r_2}^2-{r_1}^2}{{r_1}^2+{r_2}^2}\sigma_b\left[1.1+0.1\log\left(\dot{\varepsilon}\cdot s\right)\right] \\ &= \left(-0.0000029{t_b}^2+0.0018t_b+0.8\right)\frac{{r_2}^2-{r_1}^2}{{r_1}^2+{r_2}^2}\sigma_b\left[1.1+0.1\log\left(\dot{\varepsilon}\cdot s\right)\right] \end{aligned} \quad (24)$$

At the same time, the results obtained via the optimized dynamic blast pressure Equation (24), compared with the model proposed by Chen et al. [18], are shown in Figures 9–11 when t_d = 3.9 ms, 39 ms, and 390 ms, respectively. Figures 9–11 contain 16 cases for comparison. The parameters that determine the comparison results are listed in Tables A4–A6 of Appendix A, while Figures 9–11 only show the comparison results. The errors between Equation (24) and the FEM are greatly reduced, and most of the errors are less than 5%. Compared to the calculation by Equation (22), the accuracy is greatly improved. In addition, while ensuring the accuracy close to that of the prediction method in Chen et al. [18], the structure of Equation (24) is more concise. Equation (24) is a semi-empirical equation for the dynamic blast pressure of cylindrical shells subjected to explosive loads, and is able to meet the engineering requirements.

The main innovations and research significance of this paper are in three aspects: First, the explosive load in vessels is simplified as a spindle-shaped load for the dynamic blast pressure; this means of simplification has not been used in previous research in the field. Second, compared with the nonlinear load, the linear load can only be used to calculate the dynamic blast pressure with low accuracy, while in this paper the calculation accuracy after optimization is significantly higher. Third, the equations in this paper can be used as evaluation criteria to verify the accuracy of numerical calculation results. This paper provides a new method of solving the dynamic blast pressure of cylindrical shells, and could be applied in many circumstances, such as the aerospace, marine, energy, chemical, military, and security industries.

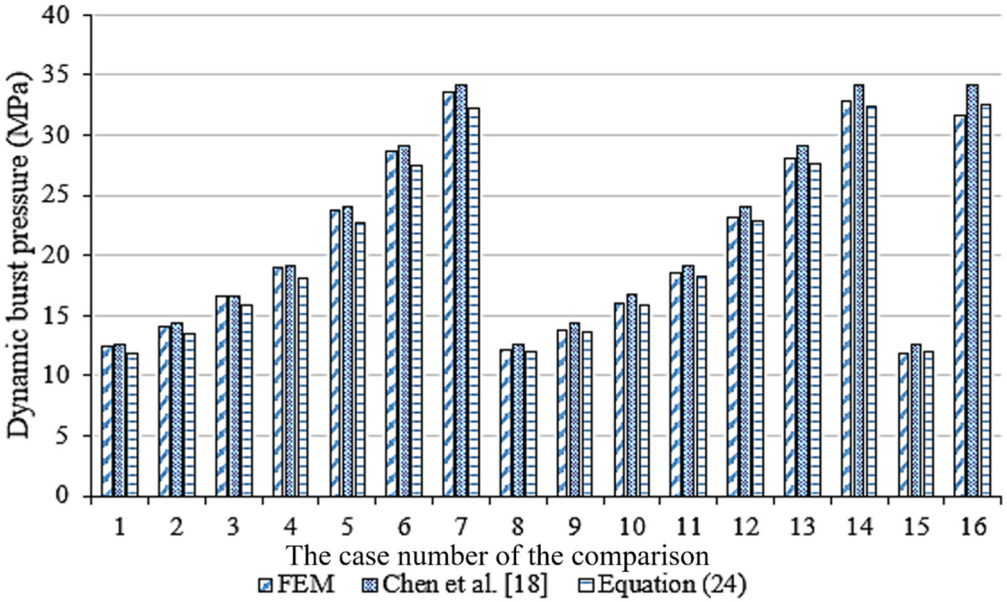

Figure 9. Comparisons between the FEM results and Equation (24), when t_d = 3.9 ms.

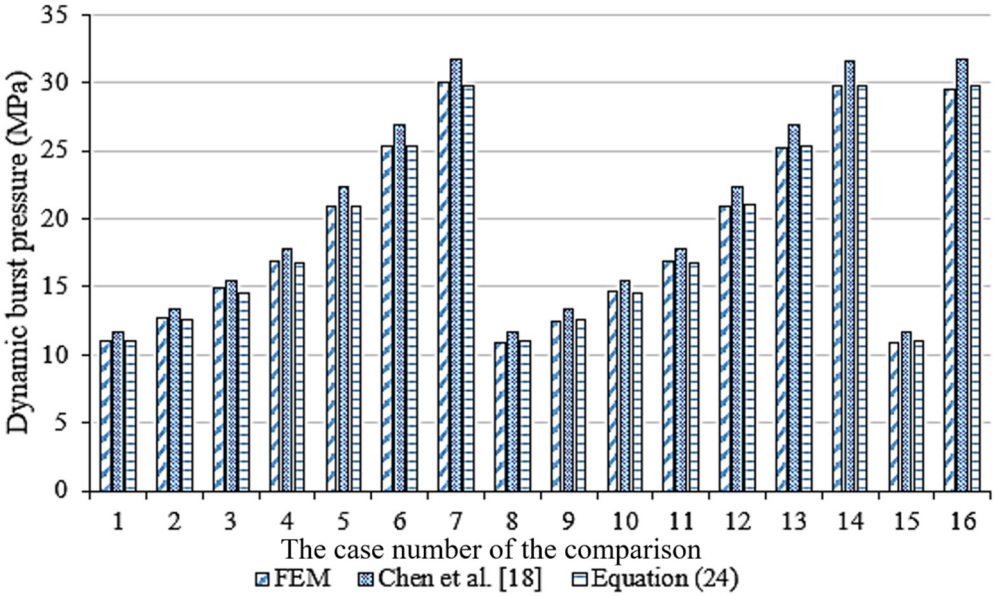

Figure 10. Comparisons between the FEM results and Equation (24), when t_d = 39 ms.

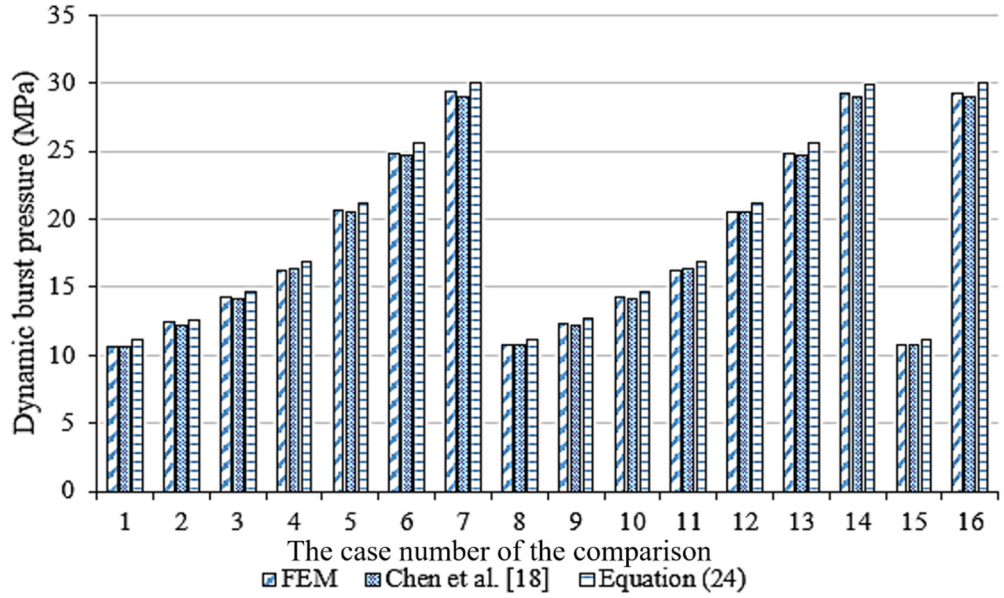

Figure 11. Comparisons between the FEM results and Equation (24), when t_d = 390 ms.

7. Conclusions

In this paper, the dynamic blast pressure of cylindrical shells subjected to non-uniform explosion loading is discussed.

(1) In terms of theory, a method to analyze the bearing capacity of pressure pipes or cylindrical shells subjected to non-uniform implosion loads is proposed. Our method expands the application of the Lame equation, which is suitable for plane problems with uniform loads. Equation (16) in this paper is used to calculate the stress distributions of cylindrical shells subjected to non-uniform implosion loads, and is able to be transformed into a Lame equation;

(2) In terms of application, a new mechanical model of cylindrical shells subjected to explosive loads is established. Unlike the previous models, this model assumes that the load is a simplified explosive load. In addition, the modified dynamic blast pressure equation of the cylindrical shell subjected to the simplified blast load is given;
(3) The accuracy of the dynamic blasting pressure equation is verified by comparing its calculation with the finite element simulation results.

This paper provides a reference benchmark for numerical calculation and approximate solution, leads to a better understanding of the failure of cylindrical shells subjected to explosive loads, and provides insights for the design and optimization of cylindrical shells.

Author Contributions: Conceptualization, Z.-F.C.; data curation, Z.S.; formal analysis, Z.S.; funding acquisition, Z.-F.C.; investigation, W.W.; methodology, H.-J.W.; project administration, Y.-X.L.; resources, Y.-X.L.; software, H.-J.W.; supervision, Z.-F.C.; validation, H.Y. and W.-M.M.; visualization, W.W.; writing—original draft, Z.-F.C. and H.-J.W.; writing—review and editing, Z.S. All authors have read and agreed to the published version of the manuscript.

Funding: This work was funded by the National Natural Science Foundation of China, grant number 51805127, and the China Postdoctoral Science Foundation, grant number 2021M693504.

Institutional Review Board Statement: Not applicable.

Informed Consent Statement: Not applicable.

Conflicts of Interest: The funders had no role in the design of the study, in the collection, analyses, or interpretation of data, in the writing of the manuscript, or in the decision to publish the results.

Appendix A

Table A1. Comparisons between the FEM results and the predictions, when t_d = 3.9 ms.

D (mm.)	T (mm.)	t_b (ms)	FEM (MPa)	Equation (22) (MPa)	Errors (%)
355.6	4.191	5.011	12.4106	14.7569	18.91
355.6	4.7752	5.236	14.0654	16.7917	19.38
355.6	5.5372	4.916	16.5475	19.5949	18.42
355.6	6.35	4.9046	19.0296	22.5252	18.37
355.6	7.9248	5.002	23.7181	28.1963	18.88
355.6	9.525	4.965	28.6824	34.0553	18.73
355.6	11.1252	4.968	33.6466	39.9484	18.73
266.7	3.14452	4.724	12.1348	14.8211	22.14
266.7	3.5814	4.79	13.7896	16.892	22.5
266.7	4.1529	4.825	15.9959	19.6193	22.65
266.7	4.7625	4.738	18.4781	22.5771	22.18
266.7	5.9436	4.738	23.1665	28.2986	22.15
266.7	7.1501	4.657	28.1308	34.2323	21.69
266.7	8.3439	4.748	32.8192	40.0693	22.09
177.8	5.5626	4.67	31.7161	40.1135	26.48
177.8	2.0955	4.426	11.8591	14.8794	25.47

Table A2. Comparisons between the FEM results and the predictions, when t_d = 39 ms.

D (mm.)	T (mm.)	t_b (ms)	FEM (MPa)	Equation (22) (MPa)	Errors (%)
355.6	4.191	40.461	11.0317	12.6961	15.09
355.6	4.7752	40.064	12.6864	14.5004	14.3
355.6	5.5372	39.626	14.8928	16.8642	13.24
355.6	6.35	40.522	16.8233	19.3495	15.02
355.6	7.9248	41.239	20.9602	24.2199	15.55
355.6	9.525	41.17	25.3729	29.2419	15.25
355.6	11.1252	40.438	30.0613	34.3513	14.27
266.7	3.1445	40.635	10.8938	12.697	16.55
266.7	3.5814	40.876	12.4106	14.4778	16.66
266.7	4.1529	39.905	14.617	16.855	15.31
266.7	4.7625	39.863	16.8233	19.3742	15.16
266.7	5.9436	40.297	20.9602	24.2635	15.76
266.7	7.1501	40.769	25.235	29.2909	16.07
266.7	8.3439	40.384	29.7855	34.3549	15.34
177.8	2.0955	40.396	10.8938	12.6977	16.56
177.8	5.5626	39.783	29.5097	34.3949	16.55

Table A3. Comparisons between the FEM results and the predictions, when t_d = 390 ms.

D (mm.)	T (mm.)	t_b (ms)	FEM (MPa)	Equation (22) (MPa)	Errors (%)
355.6	4.191	391.456	10.7007	10.4569	−2.28
355.6	4.7752	398.019	12.4106	11.9151	−3.99
355.6	5.5372	387.939	14.3412	13.8792	−3.22
355.6	6.35	395.383	16.2717	15.9237	−2.14
355.6	7.9248	388.973	20.6844	19.9898	−3.36
355.6	9.525	393.792	24.8213	24.1035	−2.89
355.6	11.1252	391.481	29.3718	28.2914	−3.68
266.7	3.1445	388.724	10.7559	10.468	−2.68
266.7	3.5814	388.998	12.2727	11.9409	−2.7
266.7	4.1529	387.14	14.3412	13.8819	−3.2
266.7	4.7625	393.439	16.2717	15.9311	−2.09
266.7	5.9436	390.747	20.5465	19.9812	−2.75
266.7	7.1501	392.35	24.8213	24.1339	−2.77
266.7	8.3439	401.02	29.234	28.2271	−3.44
177.8	2.0955	392.02	10.7559	10.4555	−2.79
177.8	5.5626	387.844	29.234	28.3163	−3.14

Table A4. Comparisons between the FEM results and the predictions, when t_d = 3.9 ms.

D (mm.)	T (mm.)	t_b (ms)	FEM (MPa)	Equation (24) (MPa)	Errors (%)
355.6	4.191	5.011	12.4106	11.9085	−4.05
355.6	4.7752	5.236	14.0654	13.5505	−3.66
355.6	5.5372	4.916	16.5475	15.8126	−4.44
355.6	6.35	4.9046	19.0296	18.1773	−4.48
355.6	7.9248	5.002	23.7181	22.7537	−4.07
355.6	9.525	4.965	28.6824	27.4818	−4.19
355.6	11.1252	4.968	33.6466	32.2374	−4.19
266.7	3.14452	4.724	12.1348	11.9603	−1.44
266.7	3.5814	4.79	13.7896	13.6314	−1.15
266.7	4.1529	4.825	15.9959	15.8323	−1.02
266.7	4.7625	4.738	18.4781	18.2192	−1.4
266.7	5.9436	4.738	23.1665	22.8363	−1.43
266.7	7.1501	4.657	28.1308	27.6246	−1.8
266.7	8.3439	4.748	32.8192	32.335	−1.48
177.8	5.5626	4.67	31.7161	11.9645	0.89
177.8	2.0955	4.426	11.8591	32.4863	2.43

Table A5. Comparisons between the FEM results and the predictions, when t_d = 39 ms.

D (mm.)	T (mm.)	t_b (ms)	FEM (MPa)	Equation (24) (MPa)	Errors (%)
355.6	4.191	40.461	11.0317	10.9921	−0.36
355.6	4.7752	40.064	12.6864	12.5543	−1.04
355.6	5.5372	39.626	14.8928	14.6008	−1.96
355.6	6.35	40.522	16.8233	16.7526	−0.42
355.6	7.9248	41.239	20.9602	20.9693	0.04
355.6	9.525	41.17	25.3729	25.3173	−0.22
355.6	11.1252	40.438	30.0613	29.741	−1.07
266.7	3.1445	40.635	10.8938	10.9929	0.91
266.7	3.5814	40.876	12.4106	12.5347	1
266.7	4.1529	39.905	14.617	14.5929	−0.16
266.7	4.7625	39.863	16.8233	16.774	−0.29
266.7	5.9436	40.297	20.9602	21.0071	0.22
266.7	7.1501	40.769	25.235	25.3597	0.49
266.7	8.3439	40.384	29.7855	29.7441	−0.14
177.8	2.0955	40.396	10.8938	11.0066	1.04
177.8	5.5626	39.783	29.5097	29.7434	0.79

Table A6. Comparisons between the FEM results and the predictions, when t_d = 390 ms.

D (mm.)	T (mm.)	t_b (ms)	FEM (MPa)	Equation (24) (MPa)	Errors (%)
355.6	4.191	391.456	10.7007	11.0938	3.67
355.6	4.7752	398.019	12.4106	12.6408	1.85
355.6	5.5372	387.939	14.3412	14.7246	2.67
355.6	6.35	395.383	16.2717	16.8936	3.82
355.6	7.9248	388.973	20.6844	21.2074	2.53
355.6	9.525	393.792	24.8213	25.5716	3.02
355.6	11.1252	391.481	29.3718	30.0146	2.19
266.7	3.1445	388.724	10.7559	11.1056	3.25
266.7	3.5814	388.998	12.2727	12.6682	3.22
266.7	4.1529	387.14	14.3412	14.7274	2.69
266.7	4.7625	393.439	16.2717	16.9015	3.87
266.7	5.9436	390.747	20.5465	21.1983	3.17
266.7	7.1501	392.35	24.8213	25.6039	3.15
266.7	8.3439	401.02	29.234	29.9464	2.44
177.8	2.0955	392.02	10.7559	11.0923	3.13
177.8	5.5626	387.844	29.234	30.041	2.76

References

1. Chatzidakis, D.; Tsompanakis, Y.; Psarropoulos, P.N. A semi-analytical approach for simulating oblique kinematic distress of offshore pipelines due to submarine landslides. *Appl. Ocean Res.* **2020**, *98*, 102111. [CrossRef]
2. Helal, M.; Huang, H.; Wang, D.; Fathallah, E. Numerical Analysis of Sandwich Composite Deep Submarine Pressure Hull Considering Failure Criteria. *J. Mar. Sci. Eng.* **2019**, *7*, 377. [CrossRef]
3. Chen, Z.; Yan, S.; Jin, Z. Dynamic burst pressure of cylindrical explosion containment vessels. *J. Press. Vessel Technol.* **2019**, *141*, 041203. [CrossRef]
4. Yao, S.; Zhang, D.; Lu, F.; Li, X. Experimental and numerical studies on the failure modes of steel cabin structure subjected to internal blast loading. *Int. J. Impact Eng.* **2017**, *110*, 279–287. [CrossRef]
5. Liu, X.; Gu, W.B.; Liu, J.Q.; Xu, J.L.; Hang, Y.M. Dynamic response of cylindrical explosion containment vessels subjected to internal blast loading. *Int. J. Impact Eng.* **2019**, *135*, 103389. [CrossRef]
6. Cheng, L.; Ji, C.; Gao, F.; Yu, Y.; Long, Y.; Zhou, Y. Deformation and damage of liquid-filled cylindrical shell composite structures subjected to repeated explosion loads: Experimental and numerical study. *Compos. Struct.* **2019**, *220*, 386–401. [CrossRef]
7. Hernandez, F.; Hao, H.; Zhang, X. On the effectiveness of ventilation to mitigate the damage of spherical chambers subjected to confined trinitrotoluene detonations. *Adv. Struct. Eng.* **2019**, *22*, 486–501. [CrossRef]
8. Cheng, S.; Li, X.; Wang, Y.; Zhou, D.; Yan, H.; Wang, Q. Analysis of Explosion Load in a Cylindrical Container With Sand Bottom. *J. Press. Vessel Technol.* **2021**, *143*, 031401. [CrossRef]
9. Davids, S.A.; Langdon, G.S.; Nurick, G.N. The influence of charge geometry on the response of partially confined right circular stainless steel cylinders subjected to blast loading. *Int. J. Impact Eng.* **2017**, *108*, 252–262. [CrossRef]

10. Sun, Q.; Dong, Q.; Yang, S. An Analytical Method to Predict Dynamic Response of Cylindrical Composite Shells Subjected to Internal Blast Loading. *J. Press. Vessel Technol.* **2019**, *141*, 061203. [CrossRef]
11. Zheng, C.; Wang, Y.; Kong, X.; Zhou, H.; Liu, H.; Wu, W. Predicting the Deflection of Square Plates Subjected to Fully Confined Blast Loading. *J. Mar. Sci. Eng.* **2020**, *8*, 1031. [CrossRef]
12. Mebarki, A. Safety of atmospheric industrial tanks: Fragility, resilience and recovery functions. *J. Loss Prev. Process Ind.* **2017**, *49*, 590–602. [CrossRef]
13. Ma, L.; Xin, J.; Hu, Y.; Zheng, J. Ductile and brittle failure assessment of containment vessels subjected to internal blast loading. *Int. J. Impact Eng.* **2013**, *52*, 28–36. [CrossRef]
14. Zheng, J.; Hu, Y.; Ma, L.; Du, Y. Delamination failure of composite containment vessels subjected to internal blast loading. *Compos. Struct.* **2015**, *130*, 29–36. [CrossRef]
15. Zheng, J.; Deng, G.; Chen, Y.; Sun, G.; Hu, Y.; Li, X.; Zhaoet, L. Experimental Investigation on Mutilayered Explosion Containment Vessels. In Proceedings of the ASME Pressure Vessels and Piping Conference, Vancouver, BC, Canada, 23–27 July 2006; pp. 1479–1484.
16. Du, Y.; Zhou, F.; Ma, L.; Zheng, J.; Xu, C.; Chen, G. Consequence analysis of premixed flammable gas explosion occurring in pipe using a coupled fluid-structure-fracture approach. *J. Loss Prev. Process Ind.* **2019**, *57*, 81–93. [CrossRef]
17. Du, Y.; Zhou, F.; Hu, W.; Zheng, L.; Ma, L.; Zheng, J. Incremental dynamic crack propagation of pipe subjected to internal gaseous detonation. *Int. J. Impact Eng.* **2020**, *142*, 103580. [CrossRef]
18. Chen, Z.; Li, X.; Wang, W.; Yang, H.; Guo, Z.; Zhu, W. Dynamic burst pressure analysis of cylindrical shells based on average shear stress yield criterion. *Thin-Walled Struct.* **2020**, *148*, 106498. [CrossRef]
19. Zheng, J.Y.; Deng, G.D.; Chen, Y.J.; Sun, G.Y.; Hu, Y.L.; Zhao, L.M.; Li, Q.M. Experimental investigation of discrete multilayered vessels under internal explosion. *Combust. Explos. Shock Waves* **2006**, *42*, 617–622. [CrossRef]
20. Esparza, E.D.; Stacy, H.; Wackerle, J. *Proof Testing of an Explosion Containment Vessel (No. LA-UR-96-2739; CONF-9608113-3)*; Los Alamos National Lab.: Los Alamos, NM, USA, 1996.
21. Hu, Y.; Liu, Q.; Bai, S.; Zhang, H. Dynamic fracture characteristics of cylindrical steel shell under internal blast loading. *Int. J. Mater. Struct. Integr.* **2014**, *8*, 291. [CrossRef]
22. Dong, Q.; Li, Q.M.; Zheng, J.Y. Interactive mechanisms between the internal blast loading and the dynamic elastic response of spherical containment vessels. *Int. J. Impact Eng.* **2010**, *37*, 349–358. [CrossRef]
23. Dong, Q.; Hu, B.Y.; Chen, S.Y.; Gu, Y. Engineering design of a multiple-use spherical explosion containment vessel subjected to internal blast loading from 25 kg TNT high explosive. *J. Press. Vessel Technol.* **2012**, *134*, 517–522. [CrossRef]
24. Liang, Y.P.; Wang, H.Z.; Ren, X.M. Analytical solution for spatially axisymmetric problem of thick-walled cylinder subjected to different linearly varying pressures along the axis and uniform pressures at two ends. *Sci. China* **2008**, *51*, 98–104. [CrossRef]
25. Basom, J.M.; Rolfe, S.T. *Fracture and Fatigue Control in Structures Applications of Fracture Mechanics*; Prentice-Hall: Englewood Cliffs, NJ, USA, 1987.
26. Chen, Z.; Zhu, W.; Di, Q.; Wang, W. Burst pressure analysis of pipes with geometric eccentricity and small thickness-to-diameter ratio. *J. Pet. Sci. Eng.* **2015**, *127*, 452–458. [CrossRef]
27. Chen, Z.; Zhu, W.; Di, Q.; Wang, W. Prediction of burst pressure of pipes with geometric eccentricity. *J. Press. Vessel Technol.* **2015**, *137*, 061201. [CrossRef]
28. Chen, Z.; Zhu, W.; Di, Q.; Li, S. Numerical and theoretical analysis of burst pressures for casings with eccentric wear. *J. Pet. Sci. Eng.* **2016**, *145*, 585–591. [CrossRef]
29. Chen, Z.; Yan, S.; Ye, H.; Shen, X.; Jin, Z. Effect of the Y/T on the burst pressure for corroded pipelines with high strength. *J. Pet. Sci. Eng.* **2017**, *157*, 760–766. [CrossRef]
30. Schreiber, J.M.; Smid, I.; Eden, T.J. Fragmentation of a steel ring under explosive loading. In Proceedings of the 1st International Conference on 3D Materials Science, Seven Springs, PA, USA, 8–12 July 2012; Springer: Cham, Switzerland, 2012; pp. 43–48.
31. Cheng, C.; Widera, G.E.O. Dynamic Burst Pressure Simulation of Cylinder-Cylinder Intersections. *J. Press. Vessel Technol.* **2010**, *132*, 011201. [CrossRef]
32. Li, D.; Hou, H.; Chen, C.; Zhu, X.; Li, M.; Yi, Q. Experimental study on the combined damage of multi-layered composite structures subjected to close-range explosion of simulated warheads. *Int. J. Impact Eng.* **2018**, *114*, 133–146. [CrossRef]
33. Cheng, C.; Widera, G.E.O. Dynamic Burst Pressure Simulation of Cylindrical Shells. *ASME J. Press. Vessel Technol.* **2009**, *131*, 061205. [CrossRef]